Microchimica Acta (2019) 186: 643
https://doi.org/10.1007/s00604-019-3750-9

ORIGINAL PAPER

Simultaneous voltammetric determination of hydroquinone and catechol by using a glassy carbon electrode modified with a ternary nanocomposite prepared from oxidized multiwalled carbon nanotubes, manganese dioxide and manganese ferrite

Sisi Chen[1] · Runmin Huang[1] · Jingang Yu[1,2] · Xinyu Jiang[1,2]

Received: 17 April 2019 / Accepted: 10 August 2019 / Published online: 23 August 2019

Abstract

An electrochemical sensor is described for simultaneous determination of hydroquinone (HQ) and catechol (CT) via differential pulse voltammetry (DPV). It is making use of a ternary composite material prepared from oxidized multiwalled carbon nanotubes, manganese dioxide (MnO_2) and manganese ferrite ($MnFe_2O_4$). The material was obtained by a one-step hydrothermal reaction and used to modify a glassy carbon electrode (GCE). The composite was characterized by Fourier transform infrared spectroscopy, X-ray powder diffraction, thermogravimetric analysis, X-ray photoelectron spectroscopy and scanning electron microscopy. The peak currents for HQ and CT are highest at 172 and 276 mV (vs. Ag/AgCl) at a pH value of 6.0. Response increases linearly in the 1–400 μM HQ and CT concentration ranges, and the detection limits are 0.64 and 0.48 μM, respectively. The modified GCE is highly selective, repeatable and reproducible. A single sensor was used to make 23 subsequent measurements, and the relative standard deviations were 1.8% and 2.3% for HQ and CT, respectively.

Keywords Electrochemical sensor · Differential pulse voltammetry · Hydrothermal reaction

Introduction

The dihydroxybenzene isomers hydroquinone (HQ), catechol (CT) and resorcinol (RE) are important intermediates in chemical raw materials, which are diffusely applied as pharmaceutical intermediates, antioxidants, dye-generating materials and reducing agents [1]. They are widely used and difficult to degrade. Thus, some health problems such as severe liver injuries, abnormal pigmentation, and hemolytic jaundice even reproductive toxicity have been triggered. Therefore, the US Environmental Protection Agency has classified these three phenolic compounds as highly toxic environmental pollutants [2]. For the sake of alleviating these hazards caused by DBIs, effective and real-time monitor of phenolic compounds such as spectrophotometry [3], capillary electrophoresis [4], chromatography analysis [5] and electrochemical analysis have been exploited.

Electrochemical analysis has been widely used due to its low-cost, simple operation and less time consumption. Unfortunately, since HQ and CT are isomers and have overlapping oxidation peaks, there are still some challenges in simultaneously distinguishing and detecting HQ and CT by using bare electrode. To solve this problem, the development of efficient and sensitive materials for simultaneously detecting HQ and CT is urgent. Various carbon based materials with excellent electronic transfer rate and good stability have been investigated. Among them, materials based on multi-walled carbon nanotubes (MWCNTs) have aroused widespread attention.

MWCNTs is a common carbon material with wonderful electron transfer rate and high sensitivity, which have been investigated for various targets such as metal ions (Pb^{2+} [6]), small biological molecules (H_2O_2, glucose [7]), organic

Electronic supplementary material The online version of this article (https://doi.org/10.1007/s00604-019-3750-9) contains supplementary material, which is available to authorized users.

✉ Xinyu Jiang
jiangxinyu@csu.edu.cn

[1] School of Chemistry and Chemical Engineering, Central South University, Changsha 410083, China

[2] Key Laboratory of Hunan Province for Water Environment and Agriculture Product Safety, Changsha 410083, China

pollutants (o-nitrophenol, p-nitrophenol [8]). In addition, it is worth noting that oxidized MWCNTs (OM) can be produced by oxidizing MWCNTs. Compared with MWCNTs, OM has more abundant functional groups (hydroxyl groups, carboxyl groups), which can strengthen interaction with target molecules and enhance its dispersion in water. Although OM holds many advantages, however, poor stability and limited catalytic activity also hinder its development in electrochemical detection. The combination of OM and other materials is an efficacious method to improve its performance.

Transition metal oxides are a class of compounds with a wide range of sources, good catalytic activity and stable structure, which are widely used in electrocatalysis and electrochemical detection. Comparing with noble metals, transition metal oxides hold absolute advantage in low costs. To boost electron transfer and hoist catalytic effect, a wide variety of metal oxides such as titanium dioxide (TiO_2) [9], zinc oxide (ZnO) [10] and manganese dioxide (MnO_2) [11] have been extensively used. It is well known that MnO_2 is considered to be one of the most attractive electrode materials [12] and is an ecological friendly economic catalyst [13]. Since the large amount of hydroxyl groups on the surface of MnO_2 can greatly improve its chemical adsorption performance [14], which further increasing the concentration of target near the electrode. Similarly, manganese ferrite ($MnFe_2O_4$), a class of spinel materials, is widely used for electrocatalysis [15], adsorption [16] and electrical storage [17] due to its good stability, unique adsorption capacity and outstanding electron transport capacity.

In this work, one-step oxidation was performed to synthesize oxidized multi-wall carbon nanotubes (OM). The ternary composite material (OM-$MnFeO_x$) was prepared by one-pot hydrothermal method, which was characterized by scanning electron microscopy (SEM), thermogravimetric analysis (TGA), X-ray diffraction (XRD), X-ray photoelectron spectroscopy (XPS) and Fourier infrared spectroscopy (FT-IR). The obtained OM-$MnFeO_x$ composite modified glass carbon electrode (OM-$MnFeO_x$/GCE) was used for simultaneous determination of HQ and CT in water sample by differential pulse voltammetry (DPV).

Experimental

Material

Potassium Permanganate ($KMnO_4$, ≥ 99.5%) was purchased from Tianjin Kermel Chemical Reagent Co., Ltd. (Tianjin, China, http://www.tjkermel.com). Anhydrous sodium sulfite (Na_2SO_3, ≥ 97%), disodium hydrogen phosphate (Na_2HPO_4, ≥ 99.0%), sodium dihydrogen phosphate (NaH_2PO_4, ≥ 99.0%), concentrated nitric acid (HNO_3, ≥ 99.0%), ferric chloride ($FeCl_3 \cdot 6H_2O$, ≥ 99.0%), anhydrous manganese Chloride ($MnCl_2$, ≥ 99.0%) were purchased from Shanghai Chemical Reagent Co., Ltd. (Shanghai, China, http://www.reagent.com.cn). Hydroquinone and catechol were acquired from Alfa Aesar (Tianjin, China, https://www.alfa.com). Phosphate buffer (PB) was prepared by mixing the stock solution of 0.1 mol·L^{-1} NaH_2PO_4 and 0.1 mol·L^{-1} Na_2HPO_4 and adjusting the pH to 6.0 by 0.1 mol·L^{-1} H_3PO_4 or 0.1 mol·L^{-1} NaOH solution. Ultrapure water was provided by a Milli-Q water purification system (Millipore, Milford, MA). All regents used were analytical grade and no further purified before use.

Synthesis of the ternary composite (OM-$MnFeO_x$)

Oxidized multi-walled carbon nanotubes (Ox-MWCNTs;bOM) was synthesized according to previous literatures [13]. The ternary composite (OM-$MnFeO_x$) was prepared by one-pot hydrothermal method: Firstly, 20 mg OM was dispersed in 10 mL ultrapure water, and then 0.114 mmol Mn^{2+} and 0.227 mmol Fe^{3+} (1:2) were added successively; After ultrasonic 10 min, the pH of mixture was adjusted to 11.5~12.5 by adding sodium hydroxide solution (12 M) drop by drop. Then the mixture was poured into 20 mL Teflon liner and heated at 180 °C for 8 h. The final product was washed several times and dried by freeze-dryer. The OM-MnO_2 was synthesized by the same method with no Fe^{3+} added.

Characterization

The Fourier transform infrared (FT-IR) was conducted on a Nicolet 6700 FT-IR spectroscopy; The XRD patterns were acquired from Rigaku D/max 2550; Field emission scanning electron microscopy (FE-SEM, MIRA3 TESCAN) was used to explore the morphology of composites; X-ray photoelectron spectroscopy (XPS, Thermo ESCALAB 250XI) was performed for determining element information of composites; Thermogravimetric analysis (TGA) was conducted on an SDT Q600 V8.0 Build 95 thermal analyzer with a heating rate 10 °C·min^{-1}.

Electrochemical experiment

Electrochemical experiments were conducted on a CHI660E Electrochemical Workstation (Chenhua Instrument Co., Ltd.) with a three- electrode system, where a platinum wire and Ag/AgCl electrode were worked as counter electrode and reference electrode, respectively. Bare or modified electrodes were acted as working electrode. Electrochemical impedance spectroscopy (EIS) was conducted in a solution containing 1.0 mM K_3 [Fe (CN) $_6$]/K_4 [Fe (CN) $_6$] and 0.1 M KCl with frequency from 1 to 10^6, amplitude = 0.005 V. Differential pulse voltammetry (DPV) was used for simultaneous determination of HQ and CT (potential range: -0.1 V ~ 0.4 V; increment: 4 mV; amplitude: 50 mV; pulse width: 0.06 s; sample width: 0.02 s; pulse period: 0.5 s).

Modification of the glassy carbon electrode (GCE)

2 mg of OM-$MnFeO_x$ was dispersed in 1 mL ultrapure water. 10 μL of modified solution was dropped on a clean surface of glassy carbon electrode (The glassy carbon electrode should be polished by 0.05 μm Al_2O_3 and washed by ultrapure water via sonication for 3 min), marked as OM-$MnFeO_x$/GCE. The other modified electrodes, including OM/GCE, OM-MnO_2/GCE and OM-$MnFe_2O_4$/GCE, were prepared as the same way.

Results and discussion

Choice of material

The ternary nanocomposite combined by OM, MnO_2 and $MnFe_2O_4$ has high specific capacitance, excellent migration rate and prominent cycle stability, and its performance is superior to that of single component and binary composite [18]. The synergistic effect of the rational integration of OM, MnO_2 and $MnFe_2O_4$ can significantly elevate their performance on electrochemical determination, which provides a platform for distinguishing and simultaneously detecting CT and HQ. The choice of OM is mainly attributed to its excellent conduction and rich oxygen-containing functional groups, which enhance interaction with target molecules by hydrogen bonding. As well as MnO_2 and $MnFe_2O_4$, hydroxyl groups on their surface improve the chemical adsorption towards HQ and CT, which is better than metal sulfides [19]. The available 4f electron orbit of Mn^{2+}/Mn^{4+} and Fe^{3+} can tremendously increase electron transfer rate on electrode surface. In addition, highly coupled ternary composite can complement each other and improve their performance.

Characterization of OM-$MnFeO_x$ composite

The phase purity and crystal structure of ternary composite was investigated by X-ray powder diffraction (XRD). The pattern is shown in Fig. S1. Some characteristic diffraction peaks of MnO_2 are indexed to (110), (200), (310), (101), (211),(301), (411), (521), (600) and (541) planes corresponding to JCPDS 44–0141 [20] and the diffraction peaks of $MnFe_2O_4$ are indexed to (111), (220), (311), (222), (400), (422), (511), (440) and (533) planes with respect to JCPDS No 74–2403 [21], which all marked on diagram. The characteristic diffraction peak of OM is marked as 002. No redundant peaks and element are found in X-ray pattern, confirming that ternary composite is relatively pure. The Fourier transform infrared spectroscopy, thermogravimetric analysis, X-ray photoelectron spectroscopy were investigated and these figures are shown in Electronic Supplementary Material (Fig. S2–4).

The surface morphology of OM-$MnFeO_x$ composite was characterized by FE-SEM. As displayed in Fig. 1, irregular MnO_2 nanospheres are grown on MWCNTs and $MnFe_2O_4$ Nano blocks are embedded among MWCNTs. The distribution of MnO_2 and $MnFe_2O_4$ is relatively uniform, providing a stable current signal for electrochemical detection. The attached growth of MnO_2 and the embedded of $MnFe_2O_4$ among MWCNTs support the synergistic effect [18].

Electrochemical performance of modified GCE

EIS and DPV were conducted on different modified GCE (Fig. 2). Unary, binary and ternary composites modified GCE were investigated. As shown in Fig. 2a, the resistance of OM/GCE, MnO_2/GCE, $MnFe_2O_4$/GCE, OM-MnO_2/GCE, OM-$MnFe_2O_4$/GCE and OM-$MnFeO_x$/GCE are

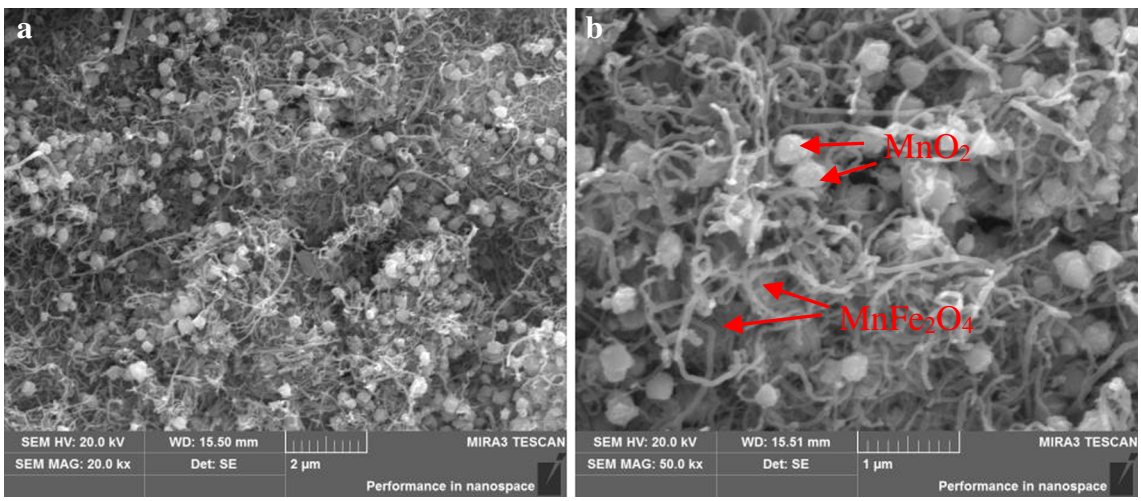

Fig. 1 The SEM images of OM-$MnFeO_x$ in low magnification (**a**) and high magnification (**b**)

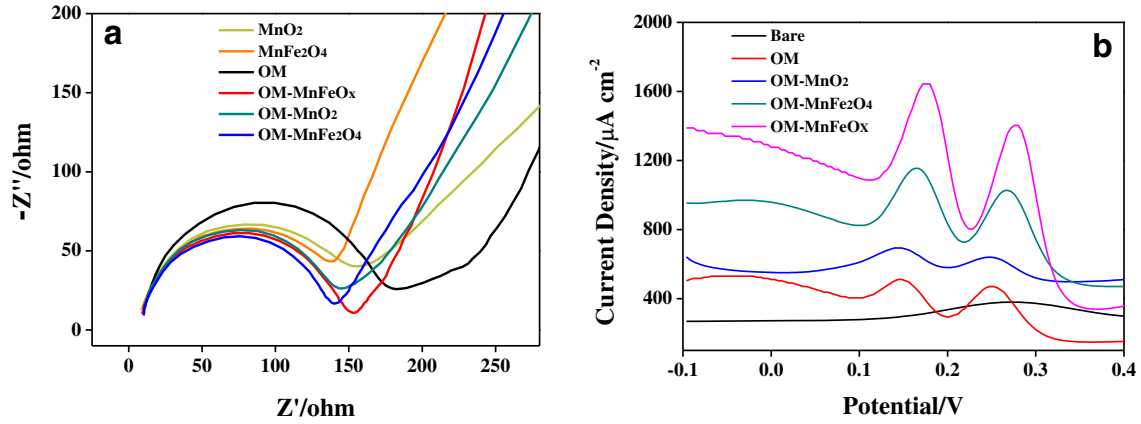

Fig. 2 **a** EIS curves of different modified GCE; **b** DPV responses of different modified GCE

similar, about 156.1 Ω, 143.4 Ω, 136.8 Ω, 130.3 Ω, 128.4 Ω and 127.6 Ω, respectively. Comparing with OM/GCE, OM-MnFeOx/GCE shows lower resistance. This indicates that OM-MnFeOx/GCE owns better electronic transmission ability and that the addition of MnO_2 and $MnFe_2O_4$ improves the electrical conductivity. Compared with unary and binary composites, ternary composite owns excellent electron transfer rate [22].

DPV responses of different electrodes are shown in Fig. 2b. The bare GCE has the poorest current signal and cannot distinguish HQ and CT. The current responses of OM/GCE, OM-MnO_2/GCE and OM-$MnFe_2O_4$/GCE are slightly lower than that of OM-$MnFeO_x$/GCE, which may attribute to the electrochemical superiority of ternary composites [23]. The peak potential difference of HQ and CT was 100 mV, 104 mV, 104 mV and 104 mV for OM/GCE, OM-MnO_2/GCE, OM-$MnFe_2O_4$/GCE and OM-$MnFeO_x$/GCE, respectively. The OM-$MnFe_2O_4$/GCE performed well in both distinction and current response. Thus, the following electrochemical detections were conducted on OM-$MnFeO_x$/GCE.

Optimization of experiment conditions

The following parameters were optimized: (a) concentration of modifier; (b) electrolyte; (c) Sample pH value. Respective data and Figures are given in the Electronic Supporting Material (Fig. S5). The following experimental conditions were found to give best results: (a) Optimal concentration of modifier: 2 mg mL^{-1}; (b) Optimal electrolyte: PB; (c) Best sample pH value: 6.

Effect of scan rate

The CV plots of modified electrode in blank buffer and targets solution are shown in Fig. 3a. The redox peak potential differences (ΔE) of HQ and CT are 31 mV and 29 mV, respectively, confirming that the electrochemical reaction at OM-$MnFeO_x$/GCE is quasi-reversible [24]. According to Nernst equation, for both HQ and CC, the number of electrons transferred during the reaction is 2, conforming well to previous research [25]. The possible electron transfer diagram is shown on Scheme S1. The chemical reaction mechanism had been investigated by changing sweep speed (from 10 $mV{\cdot}s^{-1}$ to 400 $mV{\cdot}s^{-1}$). The CV plots of HQ and CT are shown in Fig. 3b. With the increasing of scan rates, the redox peak currents increased. The anode peak current and cathode peak current of HQ and CT are proportional to the sweep speed (Fig. 3c and d). The linear equations are shown as follows:

$$\text{HQ } ipa\ (\mu\text{A}) = 0.283\ v\ (\text{mV}\cdot\text{s}^{-1}) + 2.55\ (R^2 = 0.997)$$

$$Ipc\ (\mu\text{A}) = -0.287\ v\ (\text{mV}\cdot\text{s}^{-1}) - 2.50\ (R^2 = 0.997)$$

$$\text{CT } ipa\ (\mu\text{A}) = 0.266\ v\ (\text{mV}\cdot\text{s}^{-1}) + 3.65\ (R^2 = 0.993)$$

$$Ipc\ (\mu\text{A}) = -0.227\ v\ (\text{mV}\cdot\text{s}^{-1}) - 1.37\ (R^2 = 0.997)$$

The results suggest that the reaction of HQ and CT on modified electrodes is an adsorption control process [26].

Detection of HQ and CT

Under optimal conditions, differential pulse voltammetry was used to detect HQ and CT. As shown in Fig. 4a, the oxidation peak current increased linearly with the increasing of HQ (from 1 μM to 150 μM and 150 μM to 400 μM). The linear equations are $I\ (\text{A}) = 0.424 \times C\ (\mu\text{M})$ - 0.661 ($C = 1 \sim 150\ \mu\text{M}$) and $I\ (\text{A}) = 0.193 \times C\ (\mu\text{M}) + 37.8$ ($C = 150 \sim 400\ \mu\text{M}$) with regression coefficients of 0.994 and 0.994, respectively. Two different

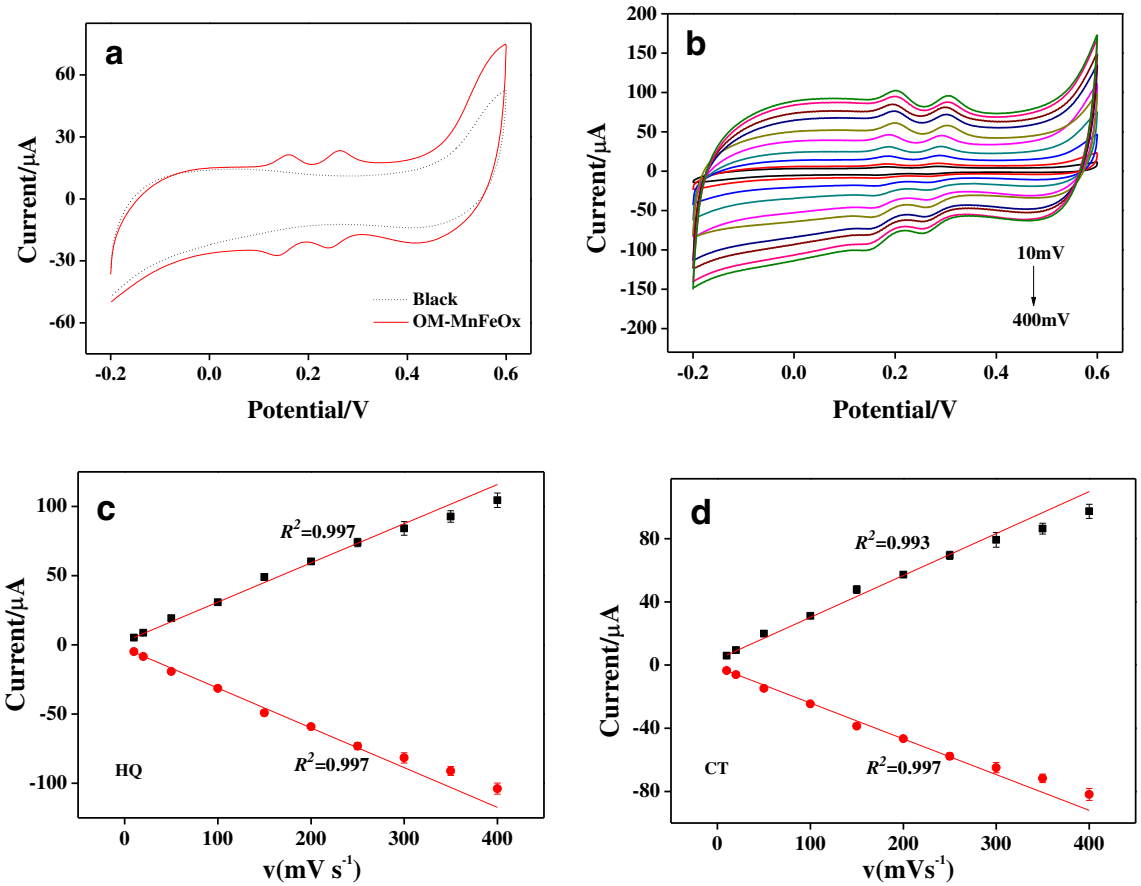

Fig. 3 **a** CV plots in blank buffer and targets solution; **b** CV plot in different scan rates (from 10 mV·s^{-1} to 400 mV·s^{-1}) under 0.1 M PB containing 0.1 mM HQ and 0.1 mM CT; **c** and **d** were curves of HQ and CT, respectively

slopes are shown on linear curve of HQ, which may attribute to different mechanism in different concentration. Under lower concentration, the adsorption effect of electrode surface dominated; once the concentration is higher, there is hydrogen bonding between HQ molecules in addition to the adsorption effect [8]. Similarly, the DPV responses of CT were investigated with the same conditions and the plots are shown in Fig. 4c, with regression equations as follows: I (A) = 0.463 × C (μM) - 0.961 (C = 1~150 μM, R^2 = 0.992) and I (A) = 0.234 × C (μM) + 31.5 (C = 150~400 μM, R^2 = 0.988). The detection limits (S/N = 3) for HQ and CT are 0.64 μM and 0.48 μM respectively, which suggests that OM-MnFeO$_x$ is applied as a suitable sensor for detecting HQ and CT. Comparing with other reported sensors, our sensor had good sensitivity (7.39 μA·μM^{-1}·cm^{-2} for HQ and 6.77 μA·μM^{-1}·cm^{-2} for CT) and stability (Table 1), which are attributed to the following three reasons: firstly, owing to its high specific surface area and well conductivity, OM is an excellent functional material for electro catalysis; Secondly, MnO_2 and $MnFe_2O_4$ are two ideal adsorbent [19], which can dramatically gather target molecules to electrode surface; Thirdly, the synergistic effect of ternary composite nanomaterial can effectively enhance electro catalytic ability.

Selectivity, stability and reproducibility

Selectivity and stable performance are two important factors that must be considered in practical application. 500 folds concentration of Na^+, K^+, NH_4^+, Cu^{2+}, Zn^{2+}, Mn^{2+}, Ca^{2+}, Mg^{2+}, Al^{3+}; 1000 folds concentration of Cl^-, NO_3^- were added into 0.1 M PB containing 0.1 mM HQ and CT. The current responses changed less than ±6.6% in the presence of these potentially interfering ions. The same concentrations of glucose (Glu), ascorbic acid (VC), Resorcinol (RE), Rutin, Luteolin (Lut), Bisphenol A (BPA), P-aminophenol (PAP), 3-nitrophenol (3-NP) and P-nitrophenol (PNP) were also added into target solution. The signal responses changed less than ±10.1%. The results confirmed that this sensor has fabulous selectivity.

Twenty-three times sequential measurements (on one modified electrode) were carried out to investigate the stability of OM-MnFeO$_x$/GCE (Fig. 5a). The relative standard deviation (RSD) of HQ and CT was 1.8% and 2.3%, respectively. The stability comparisons of different modified electrodes were

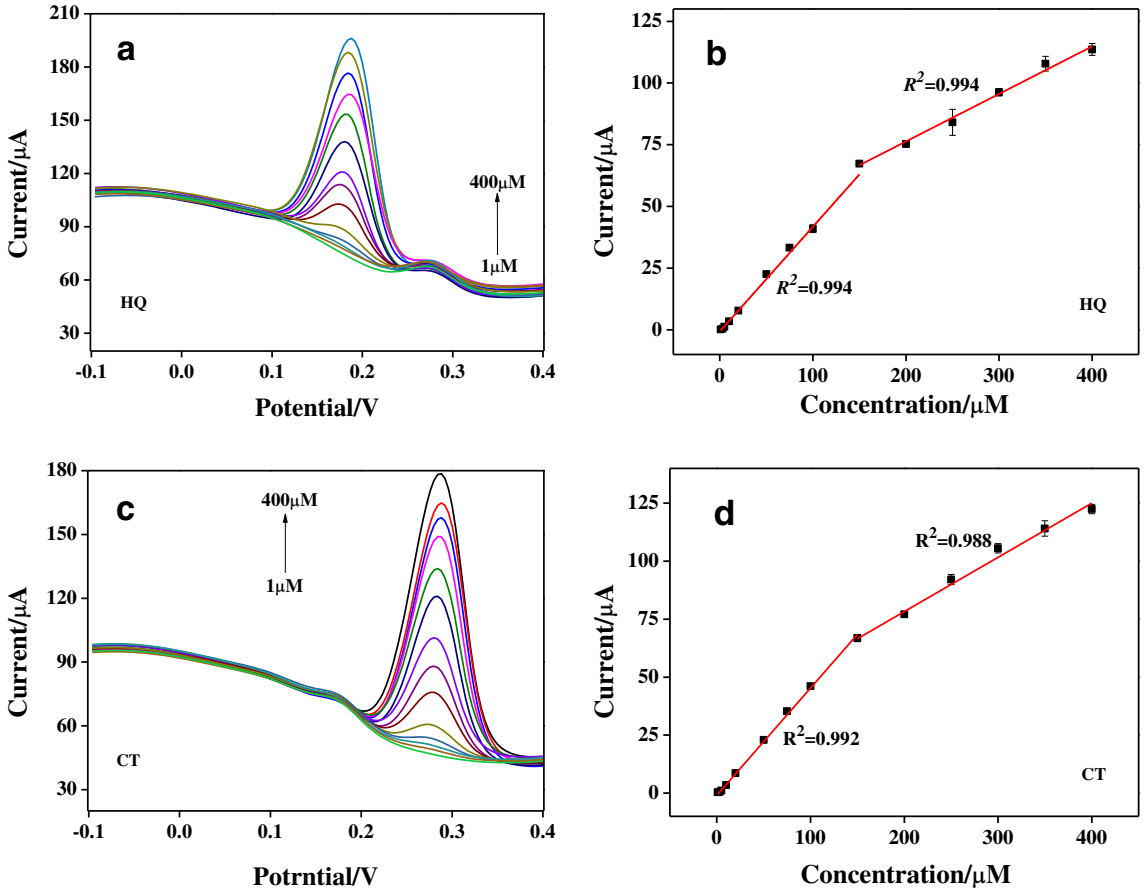

Fig. 4 **a** DPV current responses of HQ with co-existed 20 μM CT; **b** the calibration plot of HQ; **c** DPV current responses of CT with co-existed 20 μM HQ; **d** the calibration plot of CT

Table 1 Performances comparison of OM-$MnFeO_x$/GCE for the simultaneous determination of HQ and CT with other electrochemical sensors

Modified electrode		Linear range (μM)	Detection Limit (μM)	Reference
Fe/PC	HQ	0.1–120	0.014	[25]
	CT	1–120	0.033	
Graphene quantum dots	HQ	4.0–600	0.40	[27]
	CT	6.0–400	0.75	
AuNPs-MPS	HQ	10–1000	1.2	[28]
	CT	30–1000	1.1	
poly (NG B)MCPE	HQ	20–90	0.2	[29]
	CT	20–90	0.19	
PEDOT/GO	HQ	5–400	1.6	[30]
	CT	3–200	1.6	
GR/MWCNTs/$BMIMPF_6$	HQ	0.5–465,465–2900	0.1	[31]
	CT	0.2–80,80–660	0.06	
3DIPC-700	HQ	0.06–30	0.021	[32]
	CT	0.1–40	0.037	
Pal/NGE	HQ	1–50,50–90	0.8	[33]
	CT	2–50,50–100	0.13	
OM-$MnFeO_x$	HQ	1–150,150–400	0.64	This work
	CT	1–150,150–400	0.48	

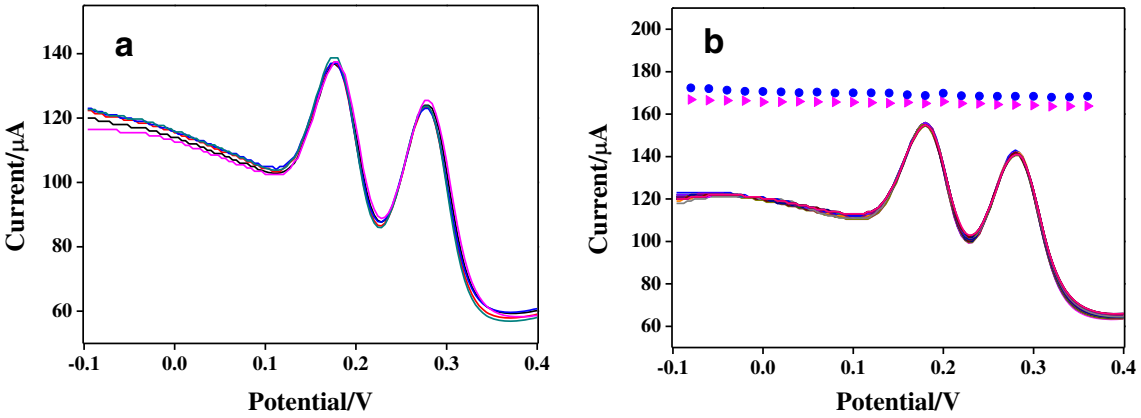

Fig. 5 **a** Continuous tests on one electrode ($n = 23$); **b** DPV responses on parallel electrodes ($n = 5$)

shown in Table S1-S3. For reproducibility evaluation, five parallel modified electrodes had been measured in 0.1 mM HQ and CT (Fig. 5b), where RSD about 2.0% for HQ and 1.9% for CT were achieved. The results showed that OM-$MnFeO_x$/GCE owned reliable stability.

Analytic application

To verify the feasibility of this method, water sample collected from a local chemical plant was analyzed at OM-$MnFeO_x$/GCE. The real sample detection was conducted by standardized recycling method. 100 μL of the actual water sample was added different concentrations of the target, and diluted to 10 mL with buffer. The results are shown in Table S4. The recovery ranges were calculated to 99.1% ~ 101.0% for HQ and 97.8% ~103.8% for CT, respectively. The results confirmed that the fabricated electrode is reliable for HQ and CT detection in actual water sample.

Conclusions

An OM-$MnFeO_x$ ternary composite material was synthesized from oxidized multi-walled carbon nanotubes and manganese ferrite and successfully applied as an electrochemical sensor for simultaneous electrochemical detection of HQ and CT. Ternary composite (OM-$MnFeO_x$), owing to its special combination method and synergistic effects, showed admirable performance on phenols oxidation. The satisfactory results were achieved by applying this sensor in real industrial waste water determination. However, this work also has some limitations. For instance, the synthesis process of materials is time consuming, and the high temperature reaction is relatively energy intensive. In addition, the morphology of ternary composite is affected by material ratio and reaction temperature. Therefore, we hope we can simplify the synthesis process and improve the electrochemical response without losing its stability in our future work.

Acknowledgments This work was supported by the National Natural Science Foundation of China (No. 21571191 and No. 51674292) and Key Laboratory of Hunan Province for Water Environment and Agriculture Product Safety (2018TP1003).

Compliance with ethical standards The author(s) declare that they have no competing interests.

References

1. Chen Y, Liu X, Zhang S, Yang L, Liu M, Zhang Y, Yao S (2017) Ultrasensitive and simultaneous detection of hydroquinone, catechol and resorcinol based on the electrochemical co-reduction prepared Au-Pd nanoflower/reduced graphene oxide nanocomposite. Electrochim Acta 231:677–685
2. Xie T, Liu Q, Shi Y, Liu Q (2006) Simultaneous determination of positional isomers of benzenediols by capillary zone electrophoresis with square wave amperometric detection. J Chromatogr A 1109:317–321
3. Fragoso S, Acena L, Guasch J, Mestres M, Busto O (2011) Quantification of phenolic compounds during red winemaking using FT-MIR spectroscopy and PLS-regression. J Agric Food Chem 59:10795–10802
4. Guan N, Zeng Z, Wang Y, Fu E, Cheng J (2000) Open tubular capillary electrochromatography in fused-silica capillaries chemically bonded with macrocyclic dioxopolyamine. Anal Chim Acta 4180:145–151
5. He JF, Yao FJ, Cui H, Li XJ, Yuan ZB (2012) Simultaneous determination of dihydroxybenzene positional isomers by capillary electrochromatography using gold nanoparticles as stationary phase. J Sep Sci 35:1003–1009
6. Wang Y, Wu Y, Xie J, Ge H, Hu X (2013) Multi-walled carbon nanotubes and metal-organic framework nanocomposites as novel hybrid electrode materials for the determination of nano-molar levels of lead in a lab-on-valve format. Analyst 138:5113–5120

7. Guzsvány V, Vajdle O, Gurdeljević M, Kónya Z (2018) Ag or Au nanoparticles decorated multiwalled carbon nanotubes coated carbon paste electrodes for Amperometric determination of H_2O_2. Top Catal 61:1350–1361
8. Li C, Wu Z, Yang H, Deng L, Chen X (2017) Reduced graphene oxide-cyclodextrin-chitosan electrochemical sensor: effective and simultaneous determination of o- and p-nitrophenols. Sensor Actuat B-Chem 251:446–454
9. Fotouhi L, Dorraji PS, Keshmiri YSS, Hamtak M (2018) Electrochemical sensor based on nanocomposite of multi-walled carbon nanotubes / TiO_2Nanoparticles in chitosan matrix for simultaneous and separate determination of Dihydroxybenzene isomers. J Electrochem Soc 165:B202–B211
10. Balram D, Lian K-Y, Sebastian N (2018) Synthesis of a functionalized multi-walled carbon nanotube decorated ruskin michelle-like ZnO nanocomposite and its application in the development of a highly sensitive hydroquinone sensor. Inorg Chem Front 5:1950–1961
11. Tang J, Jin B (2015) A voltammetric sensor based on multi-walled carbon nanotubes-MnO_2 nanowires composite film for simultaneous determination of hydroquinone and catechol. Anal Methods-UK 7:9218–9225
12. Zhang H, Wu L (2018) Na^+ intercalated manganese dioxide/MOF-derived Nanoporous carbon hybrid electrodes for supercapacitors with high rate performance and cyclic stability. J Electrochem Soc 165:2815–2823
13. Ladrak T, Smulders S, Roubeau O, Teat SJ, Gamez P, Reedijk J (2010) Manganese-based metal-organic frameworks as heterogeneous catalysts for the Cyanosilylation of acetaldehyde. Eur J Inorg Chem 2010:3804–3812
14. Luna-Lama F, Hernández-Rentero C, Caballero A, Morales J (2018) Biomass-derived carbon/γ-MnO_2 nanorods/S composites prepared by facile procedures with improved performance for Li/S batteries. Electrochim Acta 292:522–531
15. Ravindran Madhura T, Viswanathan P, Gnana kumar G, Ramaraj R (2017) Nanosheet-like manganese ferrite grown on reduced graphene oxide for non-enzymatic electrochemical sensing of hydrogen peroxide. J Electroanal Chem 792:15–22
16. Kafshgari LA, Ghorbani M, Azizi A, Agarwal S, Gupta VK (2017) Modeling and optimization of direct red 16 adsorption from aqueous solutions using nanocomposite of $MnFe_2O_4$ /MWCNTs: RSM-CCRD model. J Mol Liq 233:370–377
17. Singh G, Chandra S (2018) Electrochemical performance of $MnFe_2O_4$ nano-ferrites synthesized using thermal decomposition method. Int J Hydrogen Energ 43:4058–4066
18. Zha D, Xiong P, Wang X (2015) Strongly coupled manganese ferrite/carbon black/polyaniline hybrid for low-cost supercapacitors with high rate capability. Electrochim Acta 185:218–228
19. Liang C, Feng X, Yu J, Jiang X (2018) Facile one-step hydrothermal syntheses of graphene oxide–MnO_2 composite and their application in removing heavy metal ions. Micro Nano Lett 13:1179–1184
20. Luo J, Hu C, Meng X, Crittenden J, Qu J, Peng P (2017) Antimony removal from aqueous solution using novel α-MnO_2 nanofibers: equilibrium, kinetic, and density functional theory studies. ACS Sustain Chem Eng 5:2255–2264
21. Wu K, Hu G, Cao Y, Peng Z, Du K (2015) Facile and green synthesis of $MnFe_2O_4$/reduced graphene oxide nanocomposite as anode materials for Li-ion batteries. Mater Lett 161:178–180
22. Barai HR, Banerjee AN, Bai F, Joo SW (2018) Surface modification of titania nanotube arrays with crystalline manganese-oxide nanostructures and fabrication of hybrid electrochemical electrode for high-performance supercapacitors. J Ind Eng Chem 62:409–417
23. Xiong P, Hu C, Fan Y, Zhang W, Zhu J, Wang X (2014) Ternary manganese ferrite/graphene/polyaniline nanostructure with enhanced electrochemical capacitance performance. J Power Sources 266:384–392
24. Peng Y, Tang Z, Dong Y, Che G, Xin Z (2018) Electrochemical detection of hydroquinone based on MoS_2 /reduced graphene oxide nanocomposites. J Electroanal Chem 816:38–44
25. Huang H, Zhang J, Cheng M, Liu K, Wang X (2017) Amperometric sensing of hydroquinone using a glassy carbon electrode modified with a composite consisting of graphene and molybdenum disulfide. Microchim Acta 184(12):4803–4808
26. Xu J, Xia J, Zhang F, Wang Z (2017) An electrochemical sensor based on metal-organic framework-derived porous carbon with high degree of graphitization for electroanalysis of various substances. Electrochim Acta 251:71–80
27. Jian X, Liu X, Yang H-M, Guo M-M, Song X-L, Dai H-Y, Liang Z-H (2016) Graphene quantum dots modified glassy carbon electrode via electrostatic self-assembly strategy and its application. Electrochim Acta 190:455–462
28. Tashkhourian J, Daneshi M, Nami-Ana F, Behbahani M, Bagheri A (2016) Simultaneous determination of hydroquinone and catechol at gold nanoparticles mesoporous silica modified carbon paste electrode. J Hazard Mater 318:117–124
29. Kuskur CM, Kumara Swamy BE, Jayadevappa H (2017) Poly (naphthol green B) modified carbon paste electrode sensor for catechol and hydroquinone. J Electroanal Chem 804:99–106
30. Si W, Lei W, Zhang Y, Xia M, Wang F, Hao Q (2012) Electrodeposition of graphene oxide doped poly(3,4-ethylenedioxythiophene) film and its electrochemical sensing of catechol and hydroquinone. Electrochim Acta 85:295–301
31. Feng S, Zhang Y, Zhong Y, Li Y, Li S (2014) Simultaneous determination of hydroquinone and catechol using covalent layer-by-layer self-assembly of carboxylated-MWNTs. J Electroanal Chem 733:1–5
32. Xiang Y, li L, liu H, Shi Z, Y Tan CW, Liu Y, Wang J, Zhang S (2018) One-step synthesis of three-dimensional interconnected porous carbon and their modified electrode for simultaneous determination of hydroquinone and catechol. Sensor Actuat B-Chem 267: 302–311
33. Wu Y, Lei W, Xia M, Wang F, Li C, Zhang C, Hao Q, Zhang Y (2018) Simultaneous electrochemical sensing of hydroquinone and catechol using nanocomposite based on palygorskite and nitrogen doped graphene. Appl Clay Sci 162:38–45